

Electron Cyclotron Thruster New Modeling Results Preparation for Initial Experiments

E. Bickford Hooper
Lawrence Livermore National Laboratory

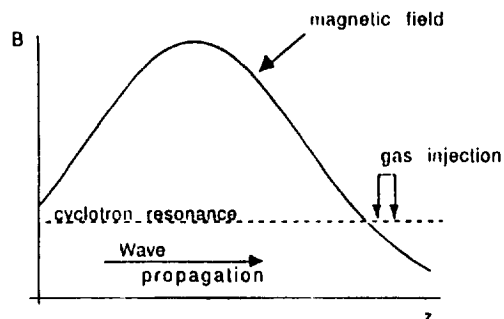


Presented at
Nuclear Propulsion Technical Interchange Meeting
NASA-LeRC Plum Brook Station
October 20-23, 1992

Whistler-Based ECRH Thruster — Concept



- A thruster using ECRH has no electrodes and, is thus less sensitive to materials problems than arc-based thrusters such as the Magneto-Plasma Dynamic (MPD) arc.



- Rear wall bombardment can be minimized, by a large mirror ratio between the resonance and peak field. (The flow across the mirror is reduced by approximately the mirror ratio from that downfield.) This:
 - o Maximizes efficiency by minimizing energy loss to the wall
 - o Maximizes lifetime by minimizing material damage

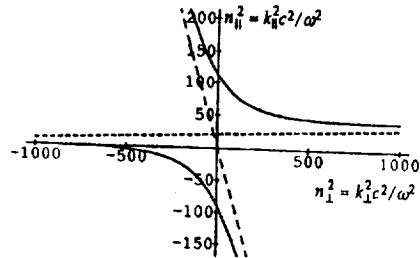
Cross-field Coupling in the Helicon Approximation



- Coupling is expected to be strongest if the magnetic field has a small gradient. Thus, we consider coupling at the peak of the magnetic mirror. There, $\omega_c/\omega, \omega_p/\omega \gg 1$. We illustrate the coupling at $\omega_c/\omega = 10, (\omega_p/\omega)^2 = 1000$. This is the helicon regime, with

$$\frac{k^2 c^2}{\omega^2} = 1 - \frac{\omega_p^2}{\omega(\omega - \omega_c \cos \theta)} = \frac{\omega_p^2}{\omega \omega_c \cos \theta}$$

- The wave characteristics can be seen from a plot of the squared parallel vs perpendicular indices of refraction



- Waves in the upper-right quadrant are propagating both along z and radially. These are the waves of interest

- There are two such waves at a given parallel index of refraction, but one is at very large perpendicular index of refraction and not of interest in the finite-radius plasma column

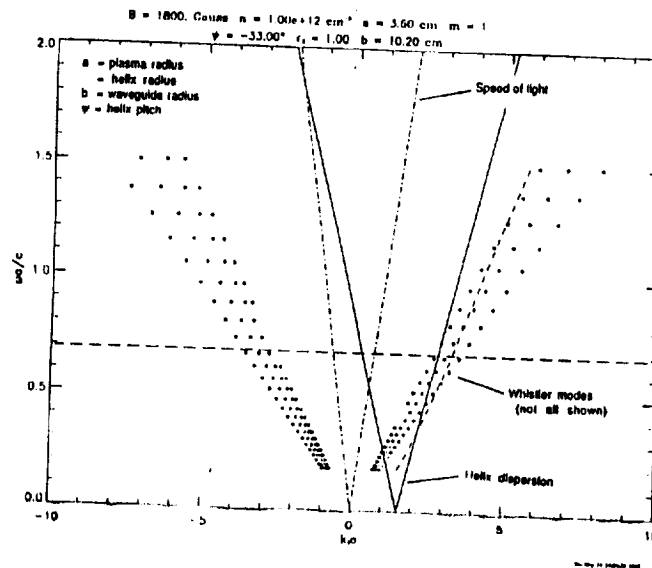
- The finite-radial geometry will pick out particular values of n_{\perp}

EBH 1/30-31/92

Wave propagation: Waveguide with helix and plasma column



- Several modes with different radial structure propagate in the system





-
- Figure 1 displays a 3x3 grid of plots showing the radial, azimuthal, and axial components of the electric field (E) and magnetic field (H) as a function of radius r (cm). The rows represent the radial (Re), azimuthal (Im), and axial (Mag) components. The columns represent the radial, azimuthal, and axial components. The plots show the real (solid line) and imaginary (dashed line) parts of the field components. The radial component (Re) shows a peak at $r=0$, while the azimuthal (Im) and axial (Mag) components show peaks at $r=0$ and $r=10$ cm. The radial component (Re) is zero at $r=10$ cm, while the azimuthal (Im) and axial (Mag) components are non-zero. The radial component (Re) is zero at $r=0$, while the azimuthal (Im) and axial (Mag) components are non-zero. The radial component (Re) is zero at $r=0$, while the azimuthal (Im) and axial (Mag) components are non-zero.
- Parameters listed on the right side of the figure:
- $\theta = 1000$ Gauss
 - $a = 5.000 \times 10^{-3}$ cm
 - $b = 2.00$ mm
 - $b = 16.00$ cm
 - $m = 1$
 - $\varphi = 35.0^\circ$
 - $n = 1.00$
 - $\alpha_1 = 4.30976 \times 10^1$
 - $\alpha_2 = 5.00014 \times 10^1$
 - $\alpha_3 = 5.000$
 - $\alpha_4 = 3.710$
 - $\alpha_5 = 5.1704 \times 10^1$
 - $\alpha_6 = 0.19232$ cm
 - $P_1 = 1.000$
 - $\alpha_7 = 0.0327 \times 10^1$
 - $\alpha_8 = 12.0704 \times 10^1$
 - $\alpha_9 = 1.000 \times 10^1$
 - $\alpha_{10} = 3.1704 \times 10^1$
 - $\alpha_{11} = -0.5270$
 - $\alpha_{12} = 0.0000$
 - $\alpha_{13} = 1.0470$
 - $\alpha_{14} = 0.0000$
 - $\alpha_{15} = -1.3630$
 - $\alpha_{16} = 0.0000$
 - $\alpha_{17} = -1.254$
 - $\alpha_{18} = 0.0000$
 - $\alpha_{19} = -1.070$
 - $\alpha_{20} = 0.001$
 - $\alpha_{21} = -2.004$
 - Repeat Interval = 15

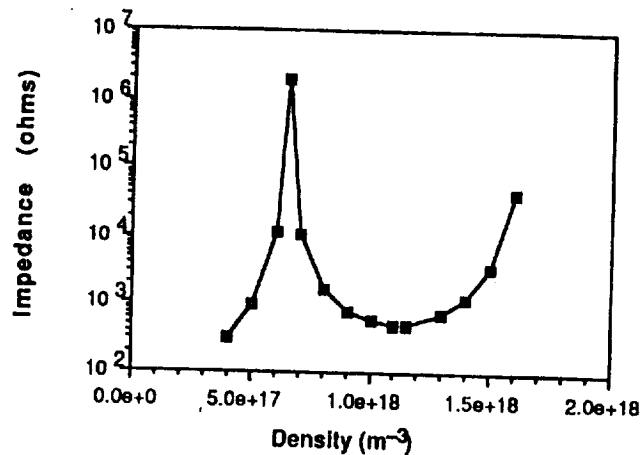


-
- Figure 1 displays a 3x3 grid of plots showing the radial, azimuthal, and axial components of the electric field (E_r , E_ϕ , E_z) and their magnitudes ($|E_r|$, $|E_\phi|$, $|E_z|$) as a function of radius r (cm). The plots are arranged in three rows and three columns. The columns are labeled 'radial', 'azimuthal', and 'axial'. The rows are labeled 'Re(E_r)', 'Im(E_r)', and 'Mag(E_r)' for the first column, and similarly for the other columns. The x-axis for all plots is r (cm), ranging from 0 to 10. The y-axis for the first column ranges from -3 to 3, for the second from -1 to 1, and for the third from 0.0 to 3.0. The plots show various oscillatory and decaying behaviors. A list of parameters is provided on the right side of the figure.
- Parameters listed on the right:
- $B = 1000$ Gauss
 - $a = 0.50 \times 10^{-1}$ cm
 - $c = 3.00$ mm
 - $b = 16.00$ mm
 - $m = 1$
 - $p = 33.00^\circ$
 - $k_z = 1.000$
 - $\omega_1 = 2.0000 \times 10^1$
 - $\omega_2 = 1.826 \times 10^1$
 - $\omega_3 = 3.200$
 - $\rho_0 = 3.151$
 - $\mu = 0.775 \times 10^{-1}$ Oer
 - $\epsilon_0 = 0.10262 \times 10^{-1}$
 - $P_1 = 1.000$
 - $\omega_1 = 15.97 \times 10^1$ Oer
 - $\omega_2 = 12.07 \times 10^1$ Oer
 - $\omega_3 = 5.166 \times 10^1$ Oer
 - $\omega_4 = 2.932 \times 10^1$ Oer
 - $\omega_5 = 0.513 \times 10^1$
 - $\text{Re } \omega^2 = 0.000 \times 10^0$
 - $\text{Re } \omega^2 = 0.003 \times 10^0$
 - $\text{Re } \omega^2 = -1.262 \times 10^0$
 - $\text{Re } \omega^2 = 0.000 \times 10^0$
 - $\text{Re } \omega^2 = 0.000 \times 10^0$
 - $\text{Re } \omega^2 = 0.000 \times 10^0$
 - $\text{Re } \omega^2 = 1.153 \times 10^0$
 - $\text{Im } \omega^2 = 0.003$
 - $\text{Im } \omega^2 = 0.270$
 - Repeat Index = 0

System impedance varies with plasma density



- The experiment is designed to allow tuning of the microwave system



Wave Absorption at the Cyclotron Resonance



- As the whistler wave approaches the cyclotron resonance, the value of k_{\parallel} becomes very large and the phase velocity becomes small

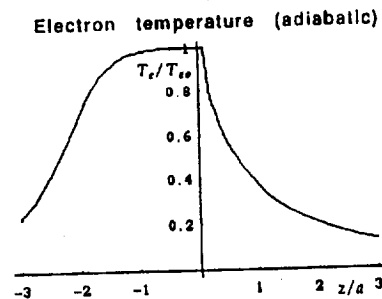
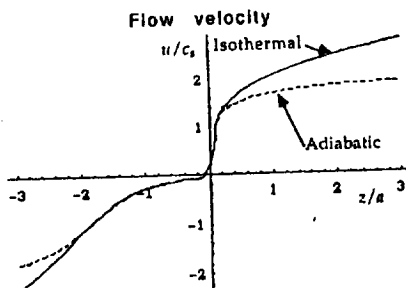
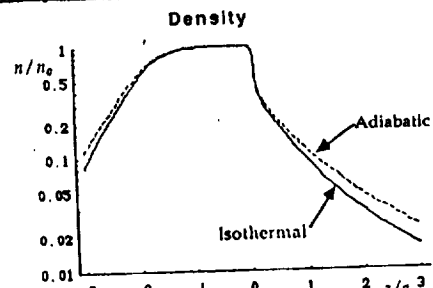
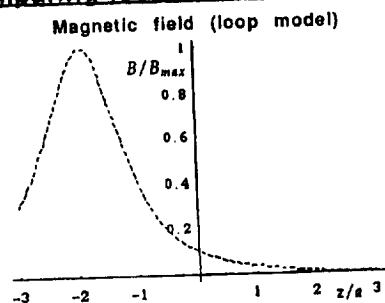
This has two favorable consequences for absorption:

- The direction of propagation becomes nearly along the field and at short wavelength so that reflection is very small
- The phase velocity becomes comparable to the thermal velocity of the particles, so that the Doppler-shifted resonance ($\omega - \omega_c - k_{\parallel} v_{\parallel} = 0$) couples to the bulk electrons
- Furthermore, there is no electromagnetic plasma mode at high density and $\omega > \omega_c$, so the wave cannot tunnel through the resonance
- Absorption is consequently nearly 100% for the whistler wave at the cyclotron resonance
- Absorption at high power will generally generate a nonthermal electron velocity distribution. Calculations are needed to quantify this and its consequences

Flow sensitivity to electron distribution function

- The isothermal and adiabatic limits illustrate the sensitivity of the flow to the thermal conductivity and thus to the electron distribution function
- For ECRH the electron distribution may be anisotropic and nonthermal in nature, with significant consequences for thermal conductivity, particle and energy flow, plasma recycling at the rear wall, etc.
- Understanding the distribution resulting from the heating, as a function of plasma density and microwave power, is thus key to predicting performance.

Comparing isothermal and adiabatic plasma flow



ECR thruster modeling: heating and plasma flow



- A particle-in-cell code – ICEPIC – has been used to model the thruster plasma heating and motion along the magnetic field
- Individual particles are followed in the guiding center approximation
 - Electrons are heated by rf with velocity-space diffusion in the quasilinear approximation
 - For the present cases, the electrons are weakly collisional
 - The ion mass is $100m_e$ to speed up calculations
- Plasma is injected on the side of a magnetic hill and heated up the hill from the injection point
- Two cases are compared

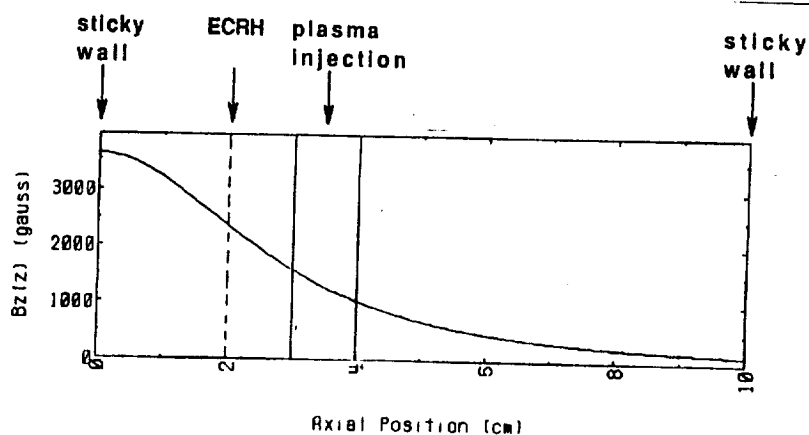
	Injected T_e	Injected T_i	ECRH
No ECRH	100 eV	5 eV	None
ECRH	5 eV	5 eV	$E_{rf} = 320$ V/cm

Geometry for PIC code model



Magnetic field strengths

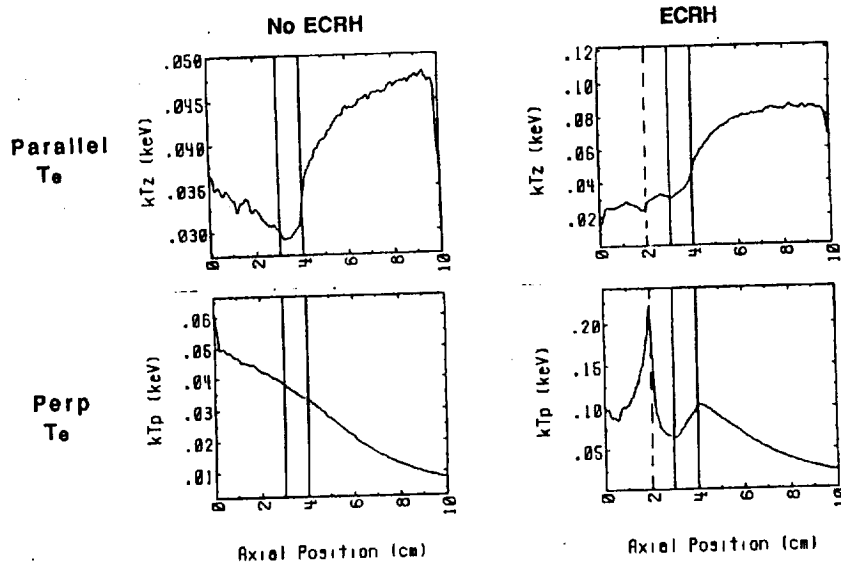
$z(\text{cm})$	0	2	3.5	10
$B(\text{gauss})$	3650	2350	1250	125
$B(0)/B$	1	1.6	2.9	29



Electron "temperature" moment in the flow



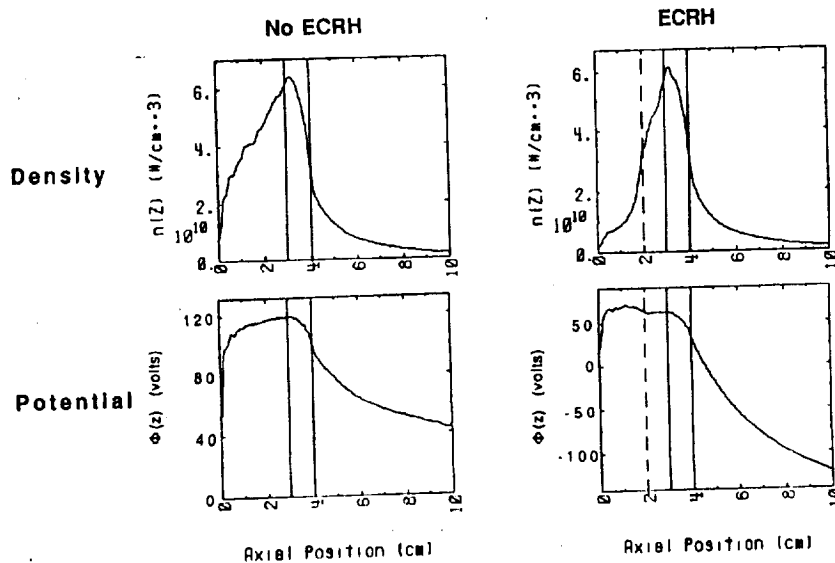
- The electrons are highly anisotropic even without ECRH
- The electron temperature is highly nonuniform along B
- Strong electron heating by ECRH is evident perpendicular to B



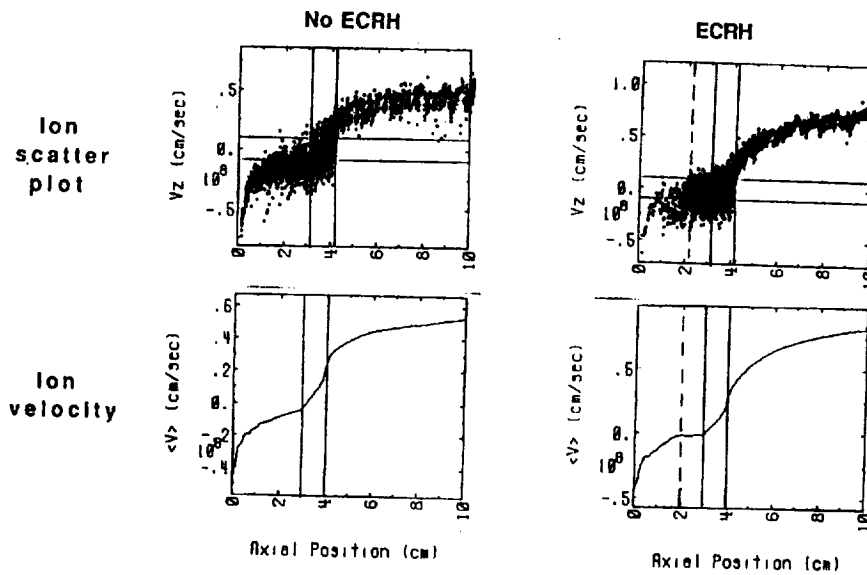
Density and potential are strongly affected by ECRH



- Note the rise in potential upfield of the ECRH. It reduces the flow of ions to balance the $\mu \partial B / \partial s$ force on the electrons and maintain quasineutrality



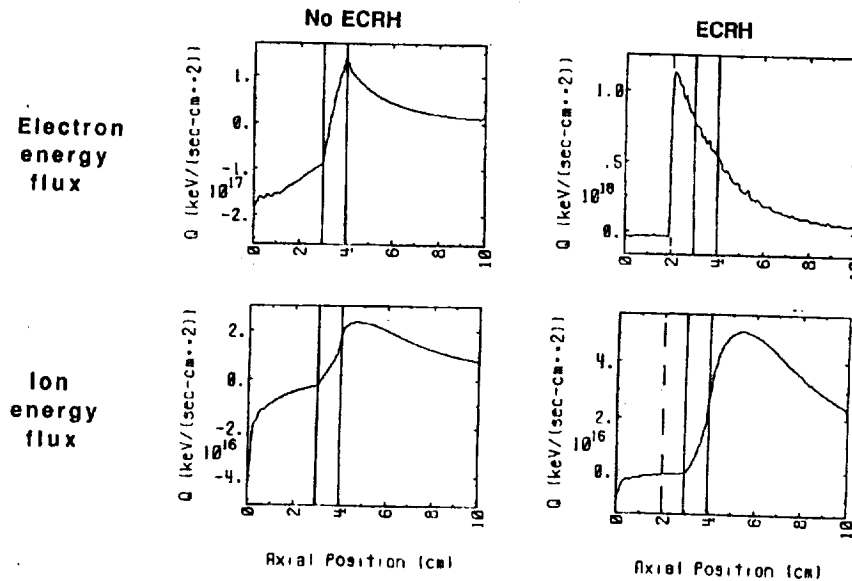
Electron energy is converted into ion flow



Energy flow up the field is suppressed by ECRH



- The total energy flow is proportional to the flux bundle area, which is a factor of 29 larger at the exit than at the magnetic field peak



Initial experimental tests: preparation



- Initial experiments will be conducted at NASA LeRC (tank 7)
 - o Space has been provided; magnets and SCR controller for pulsing microwave power have been sent to LeRC
 - o Microwave components have been delivered to LeRC
 - o Vacuum vessel, helical coupler, and gas box have been constructed and are undergoing final bench tests at LLNL
- First experiments will be directed to forming the plasma and making preliminary measurements of density, electron temperature
- Subsequent experiments will explore the details of the plasma for comparison with modeling
 - o Electron anisotropy
 - o Suppression of flow to rear wall
 - o Efficiency
- Measurements will also be made of the separation of the plasma plume from the magnetic nozzle

